16th Australasian Fluid Mechanics Conference
Crown Plaza, Gold Coast, Australia
2-7 December 2007

In-silico characterization of the flow inside a novel bioreactor for cell and tissue culture

K.Y. S. Liow[1], B. T. Tan[1], M. C. Thompson[2], K. Hourigan[2,3], and G. A. Thouas[3]

[1]School of Engineering,
Monash University, 46150 Bandar Sunway, Malaysia.
[2]Department of Mechanical Engineering,
Monash University, Victoria 3800, Australia.
[3]Division of Biological Engineering,
Monash University, Victoria 3800, Australia.

Abstract

This numerical study considers the steady, axisymmetric flow inside a novel open-top rotating-base bioreactor. The flow is simulated over a Reynolds number range that corresponds to steady axisymmetric flow. The swirling flow consists of two distinct recirculation zones, namely a primary dominant region, and a secondary recirculation bubble that is formed close to the axis of rotation. Of particular interest to tissue engineering is the stress distribution inside the bioreactor. The stress is quantified by the coordinate-independent principal stress terms, namely, the positive tensile, intermediate, and negative compressive components. The analysis indicates that there are three main regions of high strain within the bioreactor: at the rotating bottom lid; on the side walls; and at the surface close to the breakdown bubble. Finally, the local flow environment of a suspended scaffold is determined.

Keywords: bioreactor, computational fluid dynamics, principal stresses, tissue engineering

Introduction

Tissue engineering is fast emerging as an important field in biotechnology as medical researchers seek to develop *in vivo* clinical procedures for potential human tissue repair or replacement, for example, articular cartilage defects [28], cardiac cells [3]). A common device that is used in cell and tissue culture *in-vitro* is the laboratory-scaled bioreactor. To facilitate the wider use of engineered tissues, amongst others, [27] have attempted to address the bioprocess-related issue of scale-up. In order to have a successful scale-up, we would have to address one equally important issue in the development of bioreactors, that is the control and reproducibility of the environmental conditions in the bioreactor from existing laboratory-scaled low-density cultures to the high-density and/or large volume cultures (see [4], [10]). In short, a thorough understanding of the hydrodynamic and mass transport phenomena, made possible through a characterization of the different hydrodynamic effects in the bioreactor, is required.

Amongst others, some of the typical bioreactor designs that are currently in use are as follows; spinner-flask (SF) bioreactor [21], rotating concentric wall (RW) bioreactor [27] & [16], rotating-wall perfusion-flow bioreactor [1], and the wavy-walled bioreactor [2]. While there are a variety of factors to consider in the design requirements of a bioreactor (see [9]), from the fluid dynamics perspective, probably the two more important factors are the mass and momentum transport. In a comparison study of the traditional static flask, and the mixed vessels (SF and RW bioreactors) in the cultivation of articular cartilage, [25] and [26] have found that the low diffusional rates of mass transfer in the static flask has resulted in a matrix with lower collagen, high water contents, and formation of glyco-amino-glycan (GAG) only at the peripheries. In general, a mixed flask, which has higher rates of mass transfer from convection, results in an improved biochemical composition of the tissue culture, and allows for changes in the morphology of the cartilage constructs. However, it is equally clear that excessive mixing will invariably lead to high levels of fluid shear. While moderate levels of fluid shear have been shown to result in increased cell viability, high shear levels have been known to result in cell death. In this regard, the recent review on articular cartilage bioreactors by [5] suggests a preference towards low shear systems.

In this study, a numerical study of the flow- and- stress environments inside a novel bottom-wall rotating bioreactor similar to [6],[7] is presented. We would adopt the same acronym that is given to this particular mixed-flask bioreactor by [24], e.g., the rotating disc bioreactor (RDB). As alluded to by [7], the laminar RDB is proposed as a viable alternative to the turbulent SF. In particular, there is a growing interest to characterize and possibly, control the hydrodynamic conditions inside the bioreactor through the vortex breakdown (VB) theory, for example, see [11], [29], [30], [31]. The novelty of the design has led [22] to study the time-histories of the overall stress fields and to use particle tracking to predict the motion of the cell aggregates inside the flow.

The objectives of this paper are two-fold. Firstly, the numerical simulations are used to validate the experimental results of [6], [7]. Secondly, this study attempts to provide further insight into the hydrodynamic conditions inside the novel RDB, particularly near the free surface and the suspended scaffold (regions whereby there is a general difficulty in obtaining accurate experimental data). Similar to the approach of Dusting et al. (2006), this study takes on a fluid-dynamics perspective in which non-dimensional parameters are used to quantify the flow and stress fields. Often studies quantifying the effects of applying constant shear rates on different cell lines (e.g., [17],[18]) have reported shear and mixing conditions in dimensional form, and thus the results are specific to the bioreactor's physical properties as well as the cell line being cultured. In contrast, a dimensionless classification of the flow and stress fields provides significant latitude to bioreactor designers in the design and selection procedures of a scaled-up bioreactor. Reporting of the stress distribution in the fluid is done through the principal stresses which, by definition, are independent of the orientation of the axes (see [8]).

Methods

In this section, details of the numerical simulations are reported. For simplicity, the working fluid is water, and it is assumed to be Newtonian and incompressible. The schematic of the bioreactor is shown in Figure 1. The computational domain has a rectangular geometry that corresponds to an aspect ratio of $H/R = 1.5$, and a fluid-air volume ratio of 0.9:0.1. Inclusion of air above the free surface allows surface distortion. Previous simulations using a stress-free horizontal boundary has predicted subtle differences in the stress field at the free surface in comparison to the experimental results obtained by Dusting et al. (2006). The commercially available

Parameter	Symbol
Angular rotation speed	Ω
Cylinder radius	R
Cylinder height	L
Fluid height	H
Bioreactor aspect ratio	H/R
Normalized scaffold height	z/R
Normalized scaffold radius	r_s/R
Reynolds number, *Re*	$\frac{\rho\Omega R^2}{\mu}$

Table 1: Specifications of the bioreactor.

CFD software package, Fluent (version 6.3), was used to solve the incompressible Navier Stokes (NS) equations. Fluent has been used successfully for a free surface flow in the case of a submerged cylinder ([15]). Fluent provides two different formulations for linearising the discretized NS equations and consequently, solving the system of nonlinear equations, namely the *segregated* and *coupled* solver. For this study, the former was used as it was originally developed for incompressible flows. Even though the flow is expected to be steady at the Reynolds number range studied, an unsteady solver was selected. This is because the multiphase model is only available with the unsteady solver.

A first-order time-stepping scheme was used to march the simulations forward in time. The convective variables were discretized in space using the third-order MUSCL scheme while the SIMPLE algoritm was used for the pressure-velocity coupling. A spatial resolution study was conducted with the grid concentrated in regions with significant gradients (e.g., close to the wall, and on the free-surface), and a minimum spatial step-size of $\Delta x/R = 3.0 \times 10^{-4}$ was used. Temporal marching-wise, a time-step of $\Omega\Delta t/(2\pi) = 3 \times 10^{-3}$ was found to be adequate to prevent unphysical oscillations from forming at the free-surface.

As the flow is assumed be to axisymmetric, the axis boundary condition is imposed at the inner radial boundary, $r = 0$. Note, however, that finite flow asymmetries can result from small rig imperfections (see [23]). The no-slip condition is imposed at the side wall, $r = R$, and on the surfaces of the scaffold. At the fluid-air interface boundary, $z = H$, a free surface condition is imposed, and the Volume-of-Fluids (VOF) method is used.

The initial conditions are that the fluid is at rest and the rotation of the bottom disk commences abruptly at the start of the simulation, $t = 0$. The simulations are evolved in time until the solution reaches reaches steady state. Typically, the postprocessing took place after approximately 100 non-dimensionalised time units, where one time unit is the period of the lid rotation. To verify that this was sufficient, selected cases were evolved for a further 50 non-dimensionalised time units.

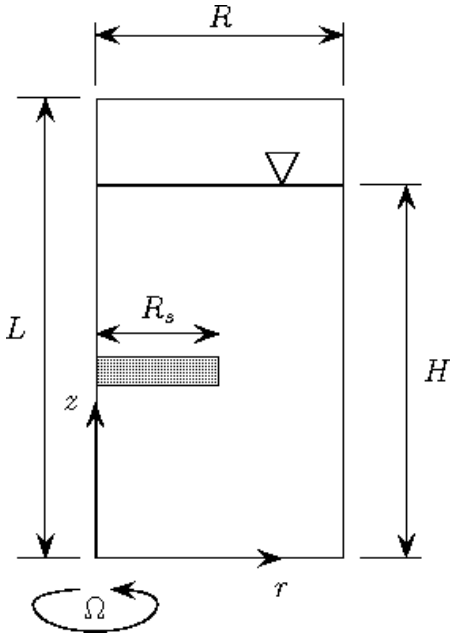

Figure 1: Schematic of the bioreactor

Numerical convergence is deemed to have been satisfied once the stress levels (monitored at the regions of interest; side-wall and VB region close to the scaffold) agrees to within 2% over every time-step.

In three-dimensional space, the stress field is a symmetric (six-component) tensor. However, it is possible to reduce the number of components to three by transforming to a rotated coordinate system. In this coordinate system, the tensor is diagonal, and the diagonal elements are called the principal stress terms. These terms define the stress environment experienced locally by a cell in the bioreactor. In order to determine the principal stress terms, it is necessary to evaluate the eigenvalues of the stress tensor, which is defined in terms of velocity gradients. This is done via a postprocessing step, implemented in *Fluent* using a User-defined Function (UDF), based on the subroutine *Jacobi* available from Numerical Recipes ([13]), to calculate the eigenvalues of the stress tensor.

Results and discussion

Flow field

The flow structure in the bioreactor at a constant aspect ratio of $H/R = 1.5$ is studied at a representative range of Reynolds numbers: $600 \leq Re \leq 1920$. As mentioned earlier, selection of this particular range assures that the flow field is steady and axisymmetric (Spohn et al. 1993). It has been widely reported in the literature (see Spohn et al. 1993, Spohn et al. 1998, Piva & Meiburg 2005) that the formation of a VB region begins with a narrow bubble developing close to the centreline. As the Reynolds number is increased, the bubble grows in size, and its upper stagnation point gradually moves toward the free surface. The closed recirculation torus is complete once the lower stagnation point reaches the free surface too. To illustrate the evolved steady flow structure and, in particular, the vortex breakdown region, axial and azimuthal velocity components, and the streamfunction, will be presented.

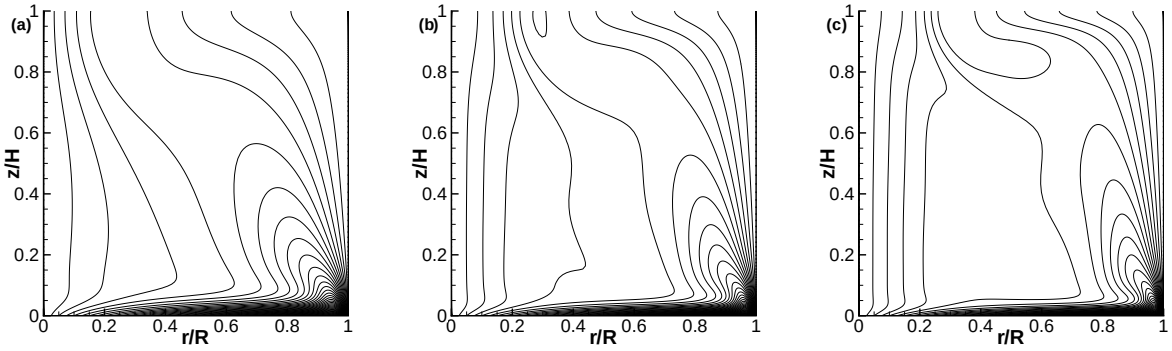

Figure 2. Contours of the non-dimensional azimuthal velocity, $v_\theta/(\Omega R)$, for (a) $Re = 780$, (b) $Re = 1350$, and (d) $Re = 1920$. Range of the contour levels is $0.0 \leq v_\theta/(\Omega R) \leq 1.0$ with Δ=0.025.

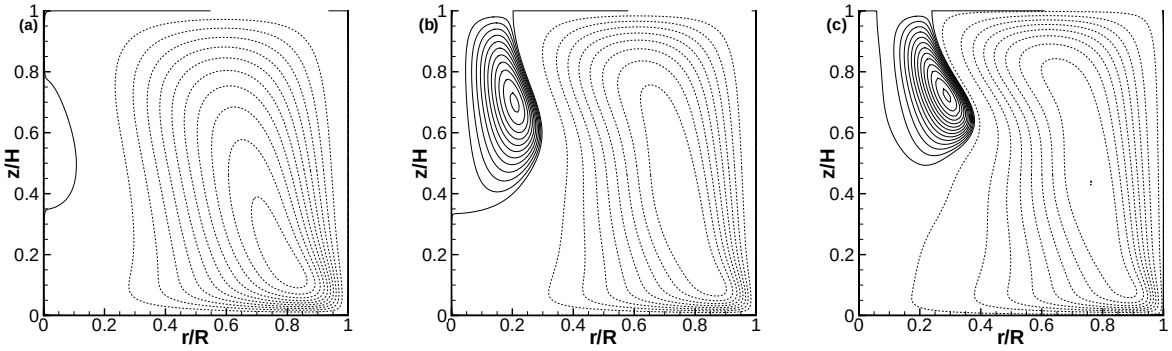

Figure 3. Contours of the normalized streamfunction, $\psi^{'} = \psi/(\Omega R^3)$, in the meridional plane for $H/R = 1.5$ at (a) $Re = 780$, (b) $Re = 1350$, and (c) $Re = 1920$. The dotted lines denote anti-clockwise recirculation, ψ_1, while the solid lines denote clock-wise recirculation, $\psi_2^{'}$. The minimum values of $\psi_1^{'}$ are as follows; (a) $(\psi_1)_{min} = -2.7 \times 10^{-4}$, (b) $(\psi_1^{'})_{min} = -3.9 \times 10^{-4}$, (c) $(\psi_1^{'})_{min} = -5.1 \times 10^{-4}$. The equally-spaced interval size is as follows; $\Delta\psi_1^{'} = 10^{-3}$, $\Delta\psi_2^{'} = 2.5 \times 10^{-5}$.

Since the flow is being driven by the rotating bottom lid, it is clear that the azimuthal velocity component should, in general, dominate over both axial and radial velocity components. Figure 2 shows the contours of the magnitude of the non-dimensional azimuthal velocity component, $v_\theta/(\Omega R)$, at $Re = 780, 1350$ and 1920. The concentration of the contour lines close to the bottom lid shows that angular momentum is being transported to the interior of the flow. We can observe from the contour plots, the formation of a nearly cylindrical core region with increasing Reynolds number, as discussed by [20]. The approximately linear increase in the vertical contour lines located in the central region indicates rigid-body rotation. Similar to the results of [20], this cylindrical core region, which is clearly observed at higher Reynolds number, spans over the entire cylinder height, H.

Figure 3 shows the contours of the streamfunction in the meridional plane as a function of increasing Reynolds number. The plots show a dominant anti-clockwise meridional recirculation generated by the centrifuging effect of the spinning bottom lid at each Reynolds number. In addition, a weaker recirculating region is also present, rotating in the opposite direction, and located close to the centreline and free surface. It is clear for $Re = 780$ that the weak and narrow *bubble* is initially embedded inside the vessel. As the Reynolds number is increased, the VB bubble moves upstream towards the free surface boundary. The contours show that the bubble has attached itself to the free surface at $Re = 900$. A widening of the VB bubble can be seen in Figure 3(c) as a result of the lower stagnation point moving upstream towards the free surface. At $Re = 1920$, there is a significant increase in the diameter of the recirculation torus at higher Reynolds number. These observations are consistent with the experimental visualizations of both [19] and [6],[7], which were recorded using dye visualisation and stereoscopic particle image velocimetry (SPIV), respectively.

Stress field

Figure 4 show the contours of the normalized tensile stress term, $\sigma_3/(\mu\Omega)$, as a function of Reynolds number. It has to be noted that since the contours positive tensile stress and the negative compressive stress reveals an almost exact mirror image, only contours of the former are reported here. Furthermore, the symmetry of σ_1 and σ_3 implies that the intermediate stress, σ_2, can be ignored as its magnitude would be close to zero because of incompressibility.

In regard to stresses that are generated along the cylinder walls, the contours show that the dominant stresses are located along the bottom wall, and a significant part of the side wall. These high stress regions can be attributed to the presence of the boundary layers, i.e., the Ekman boundary layer and the Stewartson boundary layer, respectively. By examining the azimuthal velocity contour plots (see Figure 3), it is clear that these two stress regions are strongly associated with the primary flow features. As [20] have mentioned, the momentum transfer between the wall and the interior would be mostly dependent on the cylinder aspect ratio, H/R, rather than the Reynolds number. Therefore, we would expect these two stress regions to display similar intensity levels irrespective of Reynolds number.

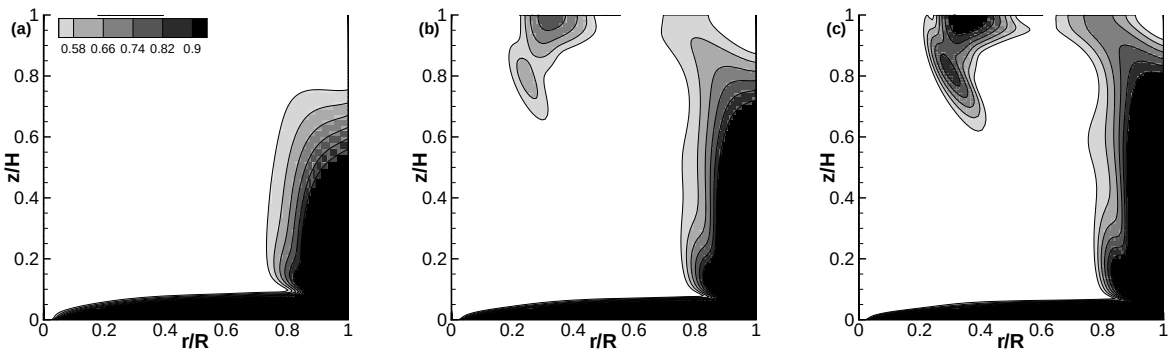

Figure 4. Contours of the non-dimensionalized principal tensile stress, $\sigma_3^{'} = \sigma_3/\mu\Omega$, at (a) $Re = 1000$, (b) $Re = 1600$, (c) $Re = 1920$.

Apart from the stresses that are formed close to the cylinder walls, a third stress region is located close to the free surface. In contrast to the cylinder wall stresses, the contours clearly show an increase in the intensity as the Reynolds number is increased. This third stress region, which originates at the approximate location of $r/R = 0.3$ at the free-surface, is clearly linked to the secondary flow features. To be more specific, this region is a direct result of the inwards travelling flow along the free-surface that is being 'forced' to separate at the radial location of $r/R \approx 0.3$. Flow separation would lead to sharp gradients, which in turn, generate stresses. Finally, perhaps of greater interest is the fact that as the Reynolds number increases, an interior stress region starts to form along the boundary separating the VB bubble from the dominant anti-clockwise recirculation region. As the Reynolds number is increased, the tail-end of this stress region slants radially outwards and is consistent with the general pattern of the VB bubble geometry.

Bioreactor with a submerged scaffold

This section considers the bioreactor configuration with a submerged scaffold. The scaffold is idealized as a stationary, solid circular disk that is placed at a fixed location of $(r,z) = (0, 0.5H)$. Three different disk sizes (normalized with respect to the cylinder radius, R) were studied, i.e., $r_s/R = 1/13, 2/13$ and 3/13. For all cases, the scaffold aspect ratio is fixed at $t_s/r_s = 0.4$ where t_s is the thickness of the scaffold, and r_s is the radius of the scaffold. The Reynolds number was kept constant at $Re = 1200$. Numerically, the solution techniques applied in this case are identical to the scaffold-free situation. Similar to the earlier case, our numerical results showed that the asymptotic solution was steady.

Figure 5 show the contours of the non-dimensionalized azimuthal velocity, $v_\theta/(\Omega R)$, as a function of aspect ratio, r_s/R. While it is clear that the presence of a scaffold would add a further parameter that can affect the flow structure, it appears that the primary flow features are still mostly dependent on the Reynolds number and the cylinder aspect ratio, H/R. In comparison with the scaffold-free case at a similar Reynolds number, there remain distinct similarities in the general structures of the primary flow, namely the transfer of angular momentum from the bottom rotating wall to the interior, the loss in momentum to the side-wall as the flow moves upstream, and finally, the presence of a centrally located, cylindrical core region.

It has been reported earlier that increasing the Reynolds number had resulted in the formation of a centrally located, cylindrical core region. Similar to what was observed in the scaffold-free case (see Figure 3), Figure 5 showed the presence of such a region, and it is clear that the azimuthal rotation rate of the core is decreasing with an increasing r_s/R. This is expected due to the loss in angular momentum from the core region to the no-slip, solid surfaces of the scaffold. The effect is not dissimilar to the viscous diffusion of a vortex core. Another flow feature of note is that while the azimuthal velocity contour lines have remained vertical across the cylinder height, H, (which implies that the central core has a rigid body rotation characteristic) for $r_s/R = 1/13, 2/13$, at the largest aspect ratio of $r_s/R = 3/13$, only the downstream region adopts a similar pattern. This observation suggests that the central core found in swirling flows is most likely to be driven by the rotating bottom wall.

The secondary flow features are shown through the contours of the normalized streamfunction, $\psi/(\rho\Omega R^3)$, in figure 6. In order to develop a better appreciation of how a scaffold affects the secondary flow features, in particular the VB bubble, the streamfunction contours of a no-scaffold case is included here. Our numerical simulations showed the presence of a steady and robust VB bubble at all three r_s/R aspect ratios, which is consistent with the results of [6],[7]. It is clear that the dominant anti-clockwise recirculation region was not being affected by the scaffold. The same cannot be said for the VB bubble, as discussed in the following paragraph.

Figure 6 also shows that while the circulation of the VB bubble remains relatively unaffected, the topology of the VB bubble undergoes rather significant changes as a result of an increasing scaffold aspect ratio, r_s/R. At $r_s/R = 1/13$, there is very little distortion of the VB bubble as the edges of the scaffold have only impinged on the outer boundaries of the VB bubble where the velocity magnitudes are comparatively small. However, as the scaffold aspect ratio is increased to $r_s/R = 2/13$, the scaffold starts to interfere with the overall VB bubble. In particular, there is a distinct narrowing in the streamfunction contours that are formed along the upper surface of the scaffold. In short, the VB bubble takes on a more compact shape as the scaffold aspect ratio is increased. The compression effect, as described by [7], is most prominent at $r_s/R = 3/13$. It is clear that the compression effect occurs even when the diameter of the scaffold is smaller than the size of the VB bubble. Probably, as a consequence of the compression effect, we would expect relatively large stress levels to be formed around the top surface of the scaffold (this will be discussed in the next paragraph). It is worthwhile mentioning that our axisymmetric simulations cannot capture the spiral pattern found downstream of the

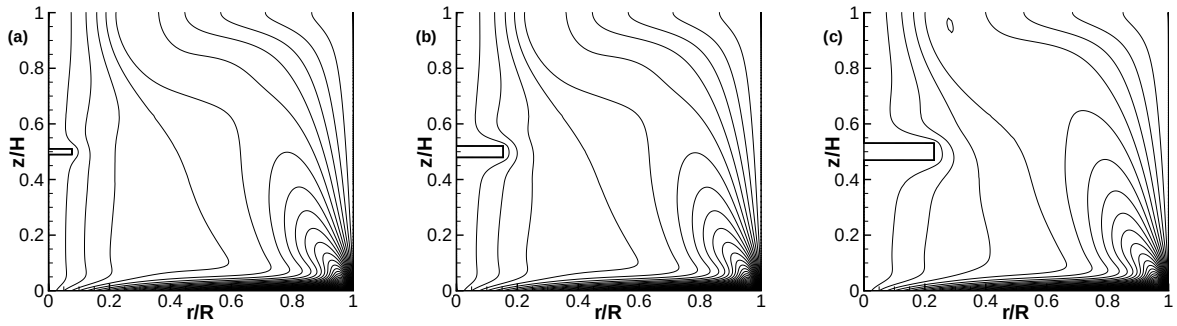

Figure 5. Contours of the normalized azimuthal velocity, $V_\theta/(\Omega R)$, at $Re = 1200$ for (a) $r_s/R = 1/13$, (b) $r_s/R = 2/13$, and (c) $r_s/R = 3/13$. The contour levels used are identical to Figure 2.

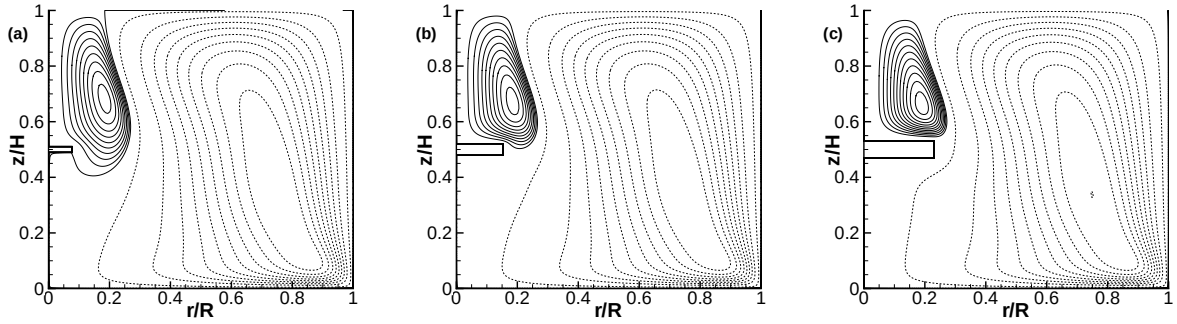

Figure 6. Contours of the normalized streamfunction, $\psi' (= \psi/(\rho\Omega R^3))$, at $Re = 1200$ for (a) $r_s/R = 1/13$, (b) $r_s/R = 2/13$, and (c) $r_s/R = 3/13$. The dotted lines denote anti-clockwise recirculation, ψ_1', while the solid lines denote clock-wise recirculation, ψ_2'. The minimum value of ψ_1' is 9.25×10^{-3}. Note that the intervals used here are identical to Figure 3.

scaffold as observed experimentally by [7]. However, it is quite possible that this particular flow pattern is a result of an asymmetry, for example, the off-centred alignment of the scaffold or rig imperfections. Future work is planned whereby 3D simulations will be performed to investigate the existence of the spiral pattern.

Figure 7 shows the contours of the non-dimensionalised principal tensile stress terms, $\sigma_3/(\mu\Omega)$, with the scaffold placed inside the bioreactor. Similar to the scaffold-free case, there are three dominant stress regions, i.e., along the bottom wall, side-wall, and the radial position of $r/R \approx 0.3$ along the free surface boundary. The stress distribution of these three regions remains unchanged as the size of the scaffold was increased, which reinforces our earlier findings that the scaffold has relatively little impact on the momentum transfer taking place along the walls, and the flow separation from the free-surface. In short, these three stress regions are associated with *Re* and H/R, rather than r_s/R. In contrast, the stresses that are formed close to the scaffold demonstrated a clear dependence on r_s/R. The peak stresses are localized around the edges of the scaffold, which is in agreement with the numerical results of Williams et al. 2002, and the experimental observations of [7]. Perhaps, of greater interest is the fact that the contours show a clear increase in both intensity and extent as the scaffold aspect ratio r_s/R, is increased. This is most likely a result of the compression effect on the VB bubble by the scaffold.

Table 2 shows the non-dimensionalised maximum and area-weighted average wall shear stresses that are found on the top and bottom surfaces of the scaffold. As expected, the maximum shear stresses occur at the edges of the scaffold where the flow has to separate at the sharp corners. The area-weighted average shear stress at the bottom surface is typically two orders of magnitude smaller than the top surface. The relatively small shear stress levels along the bottom surface is expected as Figure 7(c) shows the presence of a stagnation region downstream of the scaffold. Table 3 shows that the dimensional shear stresses on the scaffold increased with Reynolds number.

r_s/R	$(\tau'_{max})_u$	$(\tau'_{max})_l$	$(\bar{\tau'})_u$	$(\bar{\tau'})_l$
1/13	3.03	2.37	$0.54(10^{-2})$	$2.25(10^{-4})$
2/13	3.87	2.95	$2.54(10^{-2})$	$2.34(10^{-4})$
3/13	3.84	3.24	$6.21(10^{-2})$	$2.44(10^{-4})$

Table 2: Non-dimensionalised maximum wall shear stress, $\tau_{max}/(\mu\Omega)$, and area-weighted average wall shear stress, $\bar{\tau}/(\mu\Omega)$, at the upper surface, *u*, and lower surface, *l*, of the scaffold, shown here as a function of the scaffold aspect ratio, r_s/R.

Re	$(\tau)_u$ (Pa)	$(\tau)_l$ (Pa)
1200	7.13×10^{-5}	2.78×10^{-7}
1600	1.19×10^{-4}	4.39×10^{-7}
1920	1.55×10^{-4}	5.86×10^{-7}

Table 3: Dimensional area-weighted average wall shear stress, $\bar{\tau}$, at the upper and lower surfaces for the scaffold at $Re = 1200, 1600$ and 1920. Note that the scaffold aspect ratio is held constant at $r_s/R = 3/13$.

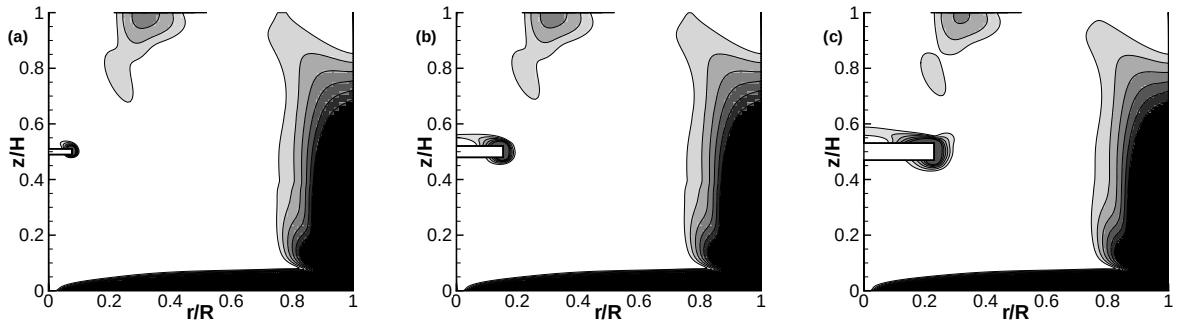

Figure 7. Contours of principal tensile stresses, $\sigma_3/(\mu\omega)$, at $Re = 1200$ for (a) $r_s/R = 1/13$, (b) $r_s/R = 2/13$, and (c) $r_s/R = 3/13$. The contour levels shown in this plot are consistent to Figure 4.

Conclusions

In this study, the momentum transport of a simple spinner-flask bioreactor is modelled using CFD. The present study is confined to the Reynolds number range over which the flow is axisymmetric, steady, and lies in the laminar regime. The axisymmetricity of the RDB offers a greater ease of characterization in the shear environment. Therefore, a logical progression from this study would be to use the basis of the RDB in achieving optimal shear rates while maintaining a 3D fluid environment that is laminar and possibly, steady. This is not unlike the concentric cylinder bioreactor configuration where the flow was confined to the laminar regime while maintaining reasonable shear rates ([16]). To that effect, we are currently expanding our scope of research to include scaffold geometrical considerations such as off-centred placements and multiple disks.

An important feature of confined swirling flow configurations is the possibility of vortex breakdown (VB). This study follows on from an experimental one by [6],[7] who had examined the flow and stress environment inside a bioreactor from a fluid dynamics viewpoint. Similar to the use of VB theory in other practical applications that have a swirling flow as a key feature, our intention is to explore the possibility of using the vortex breakdown region to provide a controlled, relatively low-stress environment for tissue growth scaffolds. A key result is the quantification of the local stress fields near a circular disk scaffold that is placed on the axis of a bioreactor. The simplicity of the design means that the flow- and- stress environments are also amenable to the design of scaled-up bioreactors.

The meridional flow shows two distinct recirculation flow patterns, i.e., a dominant, anti-clockwise primary recirculation region, and a weaker, clockwise secondary region — the VB bubble. To first order, these two regions are effectively isolated, i.e., there is no convective transport of nutrient/waste between these two regions (because of the closed streamlines; see Figure 6). However, species transport can occur through diffusion across the dividing streamlines or through opening of the bubble resulting from rig imperfections (e.g., [20],[23]. A parallel study is currently being undertaken in examining the species transport in spinner-flasks bioreactors using CFD.

The presence of the rotating bottom lid and the stationary side-wall meant that any cell aggregates that are suspended within the primary recirculation region would most likely experience large shear rates while being carried by the secondary flow as the latter is being driven radially outwards. In contrast, the stress distribution suggests that the VB region is a suitable region for the suspension of cell aggregates that requires a low shear condition. It is clear that the centrally-located vortex core region does not contribute to the stress field in the VB bubble mainly because of its rigid body rotation-like characteristic. Furthermore, the weak velocity gradients in the secondary flow (that forms the VB bubble) imply that the VB bubble is a region of relatively low shear.

In the second part of this study, a scaffold (idealized as a solid and stationary circular disk) was placed along the centreline at an axial height of $z/H = 0.5$. In terms of the stress distribution, the addition of a scaffold did not significantly alter the main stress regions that were found earlier in the scaffold-free case, e.g., along the bottom lid, side-wall, and the part of the free-surface where the inwardly travelling fluid is forced to separate. As expected, large stresses were formed on the scaffold particularly around the edges, due to the non-slip wall surface. While the scaffold had little impact on the overall dynamics of the flow i.e., the VB bubble had remained steady, it appears that topology-wise, the VB bubble has been compressed. It was found that the compression effect increased with the scaffold aspect ratio. A direct result of the compression is a distinct stagnation region lying directly underneath the scaffold. It is clear that such a region would not be conducive for suspended cell aggregates owing to its low levels of mixing and species transport.

References

[1] Begley, C.M., and Kleis, S.J., The fluid dynamics and shear environment in the NASA/JSC rotating wall perfused-vessel bioreactor, *Biotechnology and Bioengineering*, Vol. 70, No. 1, 2000, pp. 32–40.

[2] Bilgen, B., Chang-Mateu, M., and Barabino, G.A., Characterization of mixing in a novel wavy-walled bioreactor for tissue engineering, *Biotechnology and Bioengineering*, Vol. 92, No. 7, 2005, pp. 907-919.

[3] Carrier, R.L., Papadaki, M., Rupnick, M., Schoen, F.J., Bursac, N., Langer, R., Freed, L.E., and Vunjak-Novakovic, G., Cardiac tissue engineering: cell seeding, cultivation parameters, and tissue construct characterization, *Biotechnology and Bioengineering*, Vol. 64, No. 5, 1999, pp. 580-588.

[4] Croughan, M.S., Hamel, J-F., and Wang, D.I.C., Hydrodynamic effects on animal cells grown in microcarrier cul-

tures, *Biotechnology and bioengineering*, Vol. 29, 1987, pp. 130-141.

[5] Darling, E.M., and Athanasiou, K.A., Articular cartilage bioreactors and bioprocesses, *Tissue Engineering*, Vol. 9, No. 1, 2003. pp. 9–25.

[6] Dusting, J., Sheridan, J., Hourigan, K., Flows within a cylindrical cell culture bioreactor with a free-surface and a rotating base, 15th Australasian Fluid Mechanics Conference. edited by Behnia M, Lin W, McBain GD. The University of Sydney, Sydney, Australia. 13-17 December, 2004.

[7] Dusting, J., Sheridan, J., and Hourigan, K., A fluid dynamics approach to bioreactor design for cell and tissue culture, *Biotechnology and Bioengineering*, Vol. 94, 2006, pp. 1197–1208.

[8] Humphrey, J.D., Stress, strain and mechanotransduction in cells, *Trans. of the ASME J Biomechanical Engineering*, Vol. 123, 2001, pp. 638–641.

[9] Lidén, G., Understanding the bioreactor, *Bioprocess and biosystems engineering*, Vol. 24, 2002, pp. 273–279.

[10] Martin, I., Wendt, D., and Heberer, M., The role of bioreactors in tissue engineering, *Trends in Biotechnology*, Vol. 22, No. 2, 2004, pp. 80–86.

[11] Mununga, L, Hourigan, K., Thompson, M.C., Confined vortex breakdown control using a small rotating disk, *Phys Fluids*, Vol. 16, No. 12, 2004, pp. 4750–4753.

[12] Piva, M., and Meiburg, E., Steady axisymmetric flow in an open cylindrical container with a partially rotating bottom wall, *Physics of Fluids*, Vol. 17, 2005, 063603.

[13] Press, W.H., Teykolsky, S.A., Vetterling, W.T., Flannery, B.P., Numerical recipes in C++: the art of scientific computing, Cambridge, 2002, 1064 p.

[14] Raimondi M.T., Boschetti F., Migliavacca F., Cioffi M., and Dubini G., Micro fluid dynamics in three-dimensional engineered cell systems in bioreactors, Topics in Tissue Engineering, Vol. 2, Chapter 9. Eds N. Ashammakhi & R.L. Reis.

[15] Reichl, P., Hourigan, K., Thompson, M.C., Flow past a cylinder close to a free surface. *J of Fluid Mech* Vol. 533, 2005, pp. 269–296.

[16] Saini, S., and Wick, T.M., Concentric cylinder bioreactor for production of tissue engineered cartilage: effect of seeding density and hydrodynamic loading on construct development, *Biotechnol. Prog.*, Vol. 19, 2003, pp. 510–521.

[17] Smith, R.L., Donlon, B.S., Gupta, M.K., Mohtai, M., Das, P., Carter, D.R., Cooke, J., Gibbons, G., Hutchinsons, N., and Schurman, D.J., Effects of fluid-induced shear in articular chondrocyte morphology and metabolism *in vitro*. *J Orthopaedic Research*, Vol. 13, 1995, pp. 824–831.

[18] Smith, R.L., Trindade, M.C., Ikenoue, T., Mohtai, M., Das, P., Carter, D.R., Goodman, S.B., Schurman, D.J., Effects of shear stress on articular chondrocyte metabolism. *Biorheology.* Vol. 37, 2000, pp. 95–107.

[19] Spohn, A., Mory, M., and Hopfinger, E.J.,Observations of vortex breakdown in an open cylindrical container with a rotating bottom, *Exp Fluids*, Vol. 14, 1993, pp. 70–77.

[20] Spohn, A., Mory, M., and Hopfinger, E.J., Experiments on vortex breakdown in a confined flow generated by a rotating disc. *J Fluid Mech*, 370, 1998, pp. 73–99.

[21] Sucosky, P., Osorio, D.F., Brown, J.B., and Nietzel, G.P., Fluid mechanics of a spinner-flask bioreactor. *Biotechnology and bioengineering*, Vol. 85, No. 1, 2003, pp. 34-46.

[22] Tan, B.T., Liow, K., Hourigan, K., Sheridan, J., and Thompson, M.C., Predicting the flow stresses in a simplified bioreactor, In Proceedings of the Eleventh Asian Congress of Fluid Mechanics, Eds C.P. Tso, P.R. Viswanath, Y. Fukunishi and E.Cui, Kuala Lumpur, Malaysia, 2006, pp. 220–225.

[23] Thompson, M.C., Hourigan, K., The sensitivity of steady vortex breakdown bubbles in confined cylinder flows to rotating lid misalignment. *J Fluid Mech*, Vol. 496, 2003, pp. 129–138.

[24] Thouas, G.A., Sheridan, J., and Hourigan, K., A Bioreactor Model of Mouse Tumor Progression, *Journal of Biomedicine and Biotechnology*, Vol. 2007, 2007, 32754.

[25] Vunjak-Novakovic, G., Freed, L.E., Biron, R.J., and Langer, R., Effects of mixing on the composition and morphology of tissue-engineered cartilage, *AiChE J.*, Vol. 42, No. 3, 1996, pp. 850–860.

[26] Vunjak-Novakovic, G., Martin, I., Obradovic, B., Treppo, S, Grodzinsky, A.J., Langer, R, and Freed, L.E., Bioreactor cultivation conditions modulate the composition and mechanical properties of tissue-engineering cartilage, *J. Orthopaedic Research*, Vol. 17, No. 1, 1999, pp. 130–138.

[27] Williams, K.A., Saini, S., and Wick, T.M., Computational fluid dynamics modeling of steady-state momentum and mass transport in a bioreactor for cartilage tissue engineering, *Biotechnol. Prof.* Vol. 18, 2002, pp. 951–953.

[28] Wu, F., Dunkelman, N., Peterson, A., Davisson, T., Torre, R.D.L., and Jain, D., Bioreactor development for tissue-engineering cartilage, *Annals of the New York Academy of Sciences*, Vol. 875, Issue 1, 1999, pp. 405-411.

[29] Yu, P., Lee, T.S., Zeng, Y., and Low, T.H., Fluid dynamics of a micro-bioreactor for tissue engineering, *Fluid Dynamics & Materials Processing*, Vol. 1, 2005, pp. 235-246

[30] Yu, P., Lee, T.S., Zeng, Y., and Low, T.H., Effect of vortex breakdown on mass transfer in a cell culture bioreactor, *Modern Physics Letters B*, Vol. 19, Nos. 28 & 29, 1, 2005, pp. 1543-1546

[31] Yu, P., Lee, T.S., Zeng, Y., and Low, T.H., Characterization of flow behaviour in an enclosed cylinder with a partially rotating end wall, *Physics of Fluids*, Vol. 19, 2007, 057104.